

Engineering Notes

ENGINEERING NOTES are short manuscripts describing new developments or important results of a preliminary nature. These Notes should not exceed 2500 words (where a figure or table counts as 200 words). Following informal review by the Editors, they may be published within a few months of the date of receipt. Style requirements are the same as for regular contributions (see inside back cover).

Variable Structure Observer for Control Bias on Unmanned Air Vehicles

Nathan Slegers*

University of Alabama at Huntsville, Huntsville,
Alabama 35899

and

Mark Costello†

Georgia Institute of Technology, Atlanta, Georgia 30332

DOI: 10.2514/1.25321

Nomenclature

b	=	span
\bar{c}	=	chord
L, M, N	=	aerodynamic moment components in the body reference frame
p, q, r	=	components of the angular velocity of the system in the body reference frame
S	=	reference area
u, v, w	=	components of the velocity vector of the system mass center in the body frame
V_A	=	total aerodynamic velocity of the system
X, Y, Z	=	aerodynamic force components in the body reference frame
x, y, z	=	components of the position vector of the system mass center in an inertial frame
$\lambda_{\max}(M)$	=	largest eigenvalue of the matrix M
ϕ, θ, ψ	=	Euler roll, pitch, and yaw angles of the system

I. Introduction

ONE of the great selling points of military unmanned air vehicles is that they perform difficult missions in contact with the enemy while not directly endangering soldiers. These aircraft often incur damage that results in geometry changes in the aerodynamic body and wings, sensor and actuator failures, and loss of power. In some cases, loss of aircraft occurs, and in other cases, the aircraft is severely damaged to the point that the intended mission of the aircraft is compromised. Micro air vehicles are designed as expendable low-cost devices with generous tolerances, leading to relatively large variability from aircraft to aircraft. At the same time, autonomous military and homeland defense operations are being defined that require aggressive unmanned air vehicle maneuvering for flight in an urban environment, reliable operation in high winds, and tight formation flying. One of the more pervasive problems is design of the

flight control system for a highly variable aircraft. A good example that highlights this issue is control surface bias. It is often assumed that the nominal control surface position for zero control input is known. In practice, this is not the case and is particularly problematic for low-cost unmanned air vehicles. Control bias may change from flight to flight, due to landing and assembly, and even during flight, due to hinge tape heating and wear. New generation UAVs are expected to require very little human intervention and calibration of control bias for each flight is time-consuming. Integral control is often used to alleviate bias problems; however, it degrades transient response, may destabilize the system, and requires control design alteration. To eliminate this problem, a robust control surface bias observer with assured convergence properties can be added to the autopilot to create an adaptive control system.

Adaptive controllers have long been a subject of substantial research. Steinberg [1] provides a recent overview and comparison of existing adaptive control techniques. Often, adaptive flight control laws are implemented by adding an observer or online parameter estimator to an existing controller. When the parameterization is linear, static online estimation can be performed. Chandler et al. [2] proposed an adaptive controller based on a static estimation of plant parameters using constrained linear regression. This method used a batch algorithm in which a window length was used to control performance. Bodson [3] used a recursive formulation of a modified sequential least-squares algorithm (MSLS) as a parameter estimator for adaptation inside a nonlinear autopilot. MSLS has also been applied to a vertical takeoff and landing UAV [4]. Later, Shore and Bodson [5] used the MSLS algorithm for fault detection and demonstrated its real-time implementation with flight tests. In contrast to MSLS, dynamic estimation of linear parameters using a two-step Kalman filter has been investigated [6].

In general, the observation problem is nonlinear and can be solved using nonlinear observers. A commonly used nonlinear estimation technique is the well-documented extended Kalman filter (EKF) [7]. The EKF can suffer from failed convergence and sensitivity to initial parameters. For magnetometer calibration, Crassidis and Lai [8] showed that an unscented Kalman filter was more robust than a standard EKF at the cost of increased computations. Other proposed nonlinear observers, such as global linearization methods [9] and pseudolinearization [10], require transformations that are not always possible. Another approach to observer design lies in the use of a nonlinear variable structure (VS) theory that employs switching control [11,12]. The observers take a form similar to a Luenberger observer with an appended switching function. However, methods of selecting switching gains may be complicated [13]. Wang et al. [14] extended the use of a sliding mode observer for process control. Sliding observers have recently been applied extensively to induction motors [15–17].

The work reported here presents a nonlinear control surface bias observer for unmanned air vehicles. The observer uses switching control to provide robustness to sensor and modeling errors. Lyapunov theory is used to evaluate the region of practical stability when uncertainty is present. The observer is similar to sliding mode observers, with the exception that formal selection of a sliding surface is not required. The observer is compared in simulation with an EKF, and selection of observer design parameters is discussed. Finally, the nonlinear observer is tested on a small UAV on which it is shown to successfully estimate known control surface biases and achieve significant improvements in control performance.

Received 19 May 2006; revision received 28 September 2006; accepted for publication 2 October 2006. Copyright © 2006 by the American Institute of Aeronautics and Astronautics, Inc. All rights reserved. Copies of this paper may be made for personal or internal use, on condition that the copier pay the \$10.00 per-copy fee to the Copyright Clearance Center, Inc., 222 Rosewood Drive, Danvers, MA 01923; include the code \$10.00 in correspondence with the CCC.

*Assistant Professor, Department of Mechanical and Aerospace Engineering, Member AIAA.

†Sikorsky Associate Professor, School of Aerospace Engineering, Associate Fellow AIAA.

II. Unmanned Air Vehicle Model

An unmanned air vehicle can be modeled as a rigid body possessing six degrees of freedom (DOF), including three inertial position components of the system mass center as well as the three Euler orientation angles. The dynamic equations of motion are provided in Eqs. (1) and (2).

$$\begin{Bmatrix} \dot{u} \\ \dot{v} \\ \dot{w} \end{Bmatrix} = \frac{1}{m} \begin{Bmatrix} X \\ Y \\ Z \end{Bmatrix} - S_\omega \begin{Bmatrix} u \\ v \\ w \end{Bmatrix} + g \begin{Bmatrix} -s_\theta \\ s_\phi c_\theta \\ c_\phi c_\theta \end{Bmatrix} \quad (1)$$

$$\begin{Bmatrix} \dot{p} \\ \dot{q} \\ \dot{r} \end{Bmatrix} = I_T^{-1} \left(\begin{Bmatrix} L \\ M \\ N \end{Bmatrix} - S_\omega I \begin{Bmatrix} p \\ q \\ r \end{Bmatrix} \right) \quad (2)$$

where

$$S_\omega = \begin{bmatrix} 0 & -r & q \\ r & 0 & -p \\ -q & p & 0 \end{bmatrix} \quad (3)$$

$$I = \begin{bmatrix} I_{XX} & 0 & I_{XZ} \\ 0 & I_{YY} & 0 \\ I_{XZ} & 0 & I_{ZZ} \end{bmatrix} \quad (4)$$

The aerodynamic forces acting at the system mass center and the aerodynamic moments about the system mass center are given in Eqs. (5–9).

$$\begin{Bmatrix} X \\ Y \\ Z \end{Bmatrix} = \frac{1}{2} \rho S V_A^2 \begin{Bmatrix} C_{X0} + C_{X\alpha} \alpha^2 \\ C_{Y\beta} \beta \\ C_{Z0} + C_{Z\alpha} \alpha \end{Bmatrix} \quad (5)$$

$$\begin{Bmatrix} L \\ M \\ N \end{Bmatrix} = \frac{1}{2} \rho S V_A^2 \begin{Bmatrix} b C_l \\ \bar{c} C_m \\ b C_n \end{Bmatrix} \quad (6)$$

$$C_l = C_{l\beta} \beta + C_{lp} \left(\frac{b}{2V_A} \right) p + C_{l\delta_a} (\delta_a + b_a) \quad (7)$$

$$C_m = C_{m0} + C_{m\alpha} \alpha + C_{mq} \left(\frac{\bar{c}}{2V_A} \right) q + C_{m\delta_e} (\delta_e + b_e) \quad (8)$$

$$C_n = C_{n\beta} \beta + C_{nr} \left(\frac{b}{2V_A} \right) r + C_{n\delta_a} (\delta_a + b_a) \quad (9)$$

where δ_a and δ_e are aileron and elevator control, and b_a and b_e are biases in aileron and elevator control.

III. Control Bias Observer

The control bias observer estimates four states (p , q , b_a , and b_e) using the three angular velocities, total velocity V , angle of attack, and sideslip as measurements. The differential equations describing the four states to be estimated are found expanding Eq. (2) and assuming the control biases are constant.

$$\begin{aligned} \dot{p} = & \frac{\rho S V_A^2 b}{2(I_{XX} I_{ZZ} - I_{XZ}^2)} \left[I_{ZZ} (C_{l\beta} \beta + C_{l\delta_a} \delta_a) - I_{XZ} \left(C_{n\beta} \beta \right. \right. \\ & \left. \left. + C_{nr} \left(\frac{b}{2V_A} \right) + C_{n\delta_a} \delta_a \right) \right] + \left(\frac{\rho S V_A b^2 I_{ZZ} C_{lp}}{4(I_{XX} I_{ZZ} - I_{XZ}^2)} \right) p \\ & + \left(\frac{\rho S V_A b^2 (I_{ZZ} C_{l\delta_a} - I_{XZ} C_{n\delta_a})}{2(I_{XX} I_{ZZ} - I_{XZ}^2)} \right) b_a - \left(r \frac{(I_{ZZ}^2 - I_{YY} I_{ZZ} + I_{XZ}^2)}{(I_{XX} I_{ZZ} - I_{XZ}^2)} \right) q \\ & + \left(\frac{I_{XZ} (I_{YY} - I_{XX} + I_{ZZ})}{(I_{XX} I_{ZZ} - I_{XZ}^2)} \right) p q \end{aligned} \quad (10)$$

$$\dot{b}_a = 0 \quad (11)$$

$$\begin{aligned} \dot{q} = & \frac{\rho S V_A^2 \bar{c}}{2I_{YY}} [C_{m0} + C_{m\alpha} \alpha + C_{m\delta_e} \delta_e - I_{XZ} r^2] + \left(\frac{\rho S V_A \bar{c}^2 C_{mq}}{4I_{YY}} \right) q \\ & + \left(\frac{\rho S V_A^2 \bar{c} C_{m\delta_e}}{2I_{YY}} \right) b_e - \left(\frac{r(I_{XX} - I_{ZZ})}{I_{YY}} \right) p + \left(\frac{I_{XZ}}{I_{YY}} \right) p^2 \end{aligned} \quad (12)$$

$$\dot{b}_e = 0 \quad (13)$$

Errors between the actual and estimated states are defined next.

$$\mathbf{e} = \begin{Bmatrix} e_1 \\ e_2 \\ e_3 \\ e_4 \end{Bmatrix} = \begin{Bmatrix} p - \hat{p} \\ b_a - \hat{b}_a \\ q - \hat{q} \\ b_e - \hat{b}_e \end{Bmatrix} \quad (14)$$

The observer performs well if the dynamic equations for the estimated states are chosen such that the errors in Eq. (14) decrease as time increases. One possibility is to choose the estimated state differential equations as the true state differential equations in Eqs. (10–13) with two modifications: replacement of true states with their estimates and the addition of a control function. Proceeding in this manner and using identities in Eqs. (15) and (16), the error dynamics for the observer are shown in Eq. (17).

$$p q - \hat{p} \hat{q} = e_1 e_3 + \hat{p} e_3 + \hat{q} e_1 \quad (15)$$

$$p^2 - \hat{p}^2 = e_1^2 + 2\hat{p} e_1 \quad (16)$$

$$\begin{Bmatrix} \dot{e}_1 \\ \dot{e}_2 \\ \dot{e}_3 \\ \dot{e}_4 \end{Bmatrix} = \begin{Bmatrix} A e_1 - B e_3 + C e_2 + D(e_1 e_3 + \hat{p} e_3 + \hat{q} e_1) \\ 0 \\ -E e_1 + F e_3 + G e_4 + H(e_1^2 + 2e_1 \hat{p}) \\ 0 \end{Bmatrix} \quad (17)$$

$$- \begin{Bmatrix} u_{eq1} + K_1 e_1 + u_{n1} \\ u_{eq2} + u_{n2} \\ u_{eq3} + K_3 e_3 + u_{n3} \\ u_{eq4} + u_{n4} \end{Bmatrix}$$

where

$$A = \left(\frac{\rho S V_A b^2 I_{ZZ} C_{lp}}{4(I_{XX} I_{ZZ} - I_{XZ}^2)} \right) \quad (18)$$

$$B = \left(\frac{r(I_{ZZ}^2 - I_{YY} I_{ZZ} + I_{XZ}^2)}{(I_{XX} I_{ZZ} - I_{XZ}^2)} \right) \quad (19)$$

$$C = \left(\frac{\rho S V_A^2 b (I_{ZZ} C_{l\delta a} - I_{XZ} C_{n\delta a})}{2(I_{XX} I_{ZZ} - I_{XZ}^2)} \right) \quad (20)$$

$$D = \left(\frac{I_{XZ}(I_{YY} - I_{XX} + I_{ZZ})}{(I_{XX} I_{ZZ} - I_{XZ}^2)} \right) \quad (21)$$

$$E = \left(\frac{r(I_{XX} - I_{ZZ})}{I_{YY}} \right) \quad (22)$$

$$F = \left(\frac{\rho S V_A \bar{c}^2 C_{mq}}{4 I_{YY}} \right) \quad (23)$$

$$G = \left(\frac{\rho S V_A^2 \bar{c} C_{m\delta e}}{2 I_{YY}} \right) \quad (24)$$

$$H = \left(\frac{I_{XZ}}{I_{YY}} \right) \quad (25)$$

The error dynamics in Eq. (17) are clearly nonlinear; however, if the controls can be chosen so that error dynamics are well-behaved, the observer will be successful. To this end, the equivalent controls to cancel the nonlinearities are selected as follows.

$$\begin{cases} u_{eq1} \\ u_{eq2} \\ u_{eq3} \\ u_{eq4} \end{cases} = \begin{cases} Ae_1 - Be_3 + D(e_1 e_3 + \hat{p}e_3 + \hat{q}e_1) \\ (C/\sigma_1)e_1 \\ -Ee_1 + Fe_3 + H(e_1^2 + 2\hat{p}e_1) \\ (G/\sigma_3)e_3 \end{cases} \quad (26)$$

The error dynamics with the preceding controls are shown next.

$$\begin{cases} \dot{e}_1 \\ \dot{e}_2 \\ \dot{e}_3 \\ \dot{e}_4 \end{cases} = \begin{cases} -K_1 e_1 + C e_2 - u_{n1} \\ -(C/\sigma_1)e_1 - u_{n2} \\ -K_3 e_3 + G e_4 - u_{n3} \\ -(G/\sigma_3)e_3 - u_{n4} \end{cases} \quad (27)$$

Consider the general case for which the equivalent controls are not known exactly. Uncertainty can be accounted for by adding unknown but bounded disturbances into the error dynamics and limiting the initial estimates. The error dynamics can then be placed into the following nonlinear form in which ζ represents the bounded uncertainties and \sim is used to indicate estimated quantities.

$$\begin{cases} \dot{e}_1 \\ \dot{e}_2 \end{cases} = \begin{bmatrix} -K_1 & \tilde{C} \\ -\tilde{C}/\sigma_1 & 0 \end{bmatrix} \begin{cases} e_1 \\ e_2 \end{cases} + \begin{cases} \zeta_1(e, t) \\ \zeta_2(e, t) \end{cases} - \begin{cases} u_{n1} \\ u_{n2} \end{cases} \quad (28)$$

$$\begin{cases} \dot{e}_3 \\ \dot{e}_4 \end{cases} = \begin{bmatrix} -K_3 & \tilde{G} \\ -\tilde{G}/\sigma_3 & 0 \end{bmatrix} \begin{cases} e_3 \\ e_4 \end{cases} + \begin{cases} \zeta_3(e, t) \\ \zeta_4(e, t) \end{cases} - \begin{cases} u_{n3} \\ u_{n4} \end{cases} \quad (29)$$

The two systems have identical form: $\dot{s} = As + \zeta - U$, where s is the two-element state vector. Let P represent the positive definite solution to the following Lyapunov.

$$PA + A^T P = -Q \quad (30)$$

Consider the function $V = s^T P s$ and the following control U .

$$U = \begin{cases} K_{s1} \text{sign}(s_1) \\ -K_{s1} \frac{p_{12}}{p_{22}} \text{sign}(s_2) \end{cases} \quad (31)$$

It is straightforward to show that V has the following bounds on its

derivative [18].

$$\dot{V} \leq -s^T Q s - 2 \det(P) p_{22} K_{s1} |s_1| + \delta \|s\| \|\zeta\| \quad (32)$$

where $\delta = 2\sqrt{\lambda_{\max}(PP)}$. The first two terms in Eq. (32) are always less than zero. A region R_δ exists near the origin for $s \notin R_\delta$, $\dot{V} < 0$. Therefore, the system is ultimately bounded with respect to the region R_δ . The size of R_δ is determined by selection of P , Q , and K_{s1} , with the region area decreasing as the switching gain K_{s1} is increased. An additional design consideration is to have the ratio p_{12}/p_{22} be small so that high gain switching does not occur on the desired bias observations. Combining the control elements of Eqs. (17), (26), and (31) the bias observer takes the final form shown in Eqs. (33–36).

$$\begin{aligned} \dot{\hat{p}} = & \frac{\rho S V_A^2 b}{2(I_{XX} I_{ZZ} - I_{XZ}^2)} \left[I_{ZZ}(C_{l\beta} \beta + C_{l\delta a} \delta_a) - I_{XZ} \left(C_{n\beta} \beta \right. \right. \\ & \left. \left. + C_{nr} \left(\frac{b}{2V_A} \right) + C_{n\delta a} \delta_a \right) \right] + Ap - Bq + Cb_a + Dpq \\ & + K_1(p - \hat{p}) + K_{s1} \text{sign}(p - \hat{p}) \end{aligned} \quad (33)$$

$$\dot{\hat{b}}_a = (C/\sigma_1)(p - \hat{p}) - K_{s1} \frac{p_{12}^1}{p_{22}^1} \text{sign}(p - \hat{p}) \quad (34)$$

$$\begin{aligned} \dot{\hat{q}} = & \frac{\rho S V_A^2 \bar{c}}{2 I_{YY}} [C_{m0} + C_{m\alpha} \alpha + C_{m\delta e} \delta_e - I_{XZ} r^2] - Ep + Fq \\ & + G\hat{b}_e + Hp^2 + K_3(q - \hat{q}) + K_{s3} \text{sign}(q - \hat{q}) \end{aligned} \quad (35)$$

$$\dot{\hat{b}}_e = (G/\sigma_3)(q - \hat{q}) - K_{s1} \frac{p_{12}^2}{p_{22}^2} \text{sign}(q - \hat{q}) \quad (36)$$

IV. Results

The control bias observer is simulated on a rudderless unmanned air vehicle, with physical properties given in Table 1 and the aerodynamic coefficient given in Table 2. The vehicle model and observer are numerically integrated using a fourth-order Runge–Kutta algorithm. The observer is updated at 0.125-s intervals. In all simulations, the true aileron and elevator biases are 1.5 and 3.0 deg, respectively. Initial estimates of the aileron and elevator biases are taken as -1.5 and -3.0 deg. A proportional-derivative controller with knowledge of the estimated biases is used on the UAV to track a step increase in altitude of 30 m, whereas a 3-deg sinusoidal aileron is applied at a frequency of $\pi/8$ rad/s. The proportional observer gains K_1 and K_3 are 2, whereas the switching gains K_{s1} and K_{s3} are 0.25. Parameters σ_1 and σ_3 are chosen as 842 and 782, respectively. Finally, the matrices Q are chosen so that the solution to the Lyapunov equation for the systems in Eqs. (28) and (29) yields $p_{12}^1/p_{22}^1 = 0.0042$ and $p_{12}^2/p_{22}^2 = 0.0047$.

The VS observer and UAV described earlier are implemented initially with no sensor noise. The results are shown in Figs. 1 and 2.

Table 1 UAV physical parameters

Variable	Value	Units
Weights	28.6	N
S	0.38	m ²
b	1.3	m
\bar{c}	0.22	m
I_{XX}	0.093	kg · m ²
I_{YY}	0.265	kg · m ²
I_{ZZ}	0.352	kg · m ²
I_{XZ}	0.0	kg · m ²

Table 2 UAV aerodynamic coefficients

Parameter	Value
$C_{l\beta}$	-0.005
C_{lp}	-0.362
$C_{l\delta a}$	-0.043
C_{m0}	0.031
$C_{m\alpha}$	-0.625
C_{mq}	-8.43
$C_{m\delta e}$	-0.817
$C_{n\beta}$	0.002
C_{nr}	-0.051
$C_{n\delta a}$	0.0

An EKF based on the dynamic model described in Eqs. (10–14) is also implemented, with results shown along with the VS observer for comparison. In Fig. 1 the VS aileron bias converges within 5% of the true aileron bias in 10 s. The EKF converges in 3 s, however, oscillations 0.25 deg above and below the true bias persist because of the continuous motion on the UAV. Figure 2 shows the elevator bias for which both the VS observer and EKF converge to the true bias within 5 s. Unlike the aileron bias, the EKF elevator bias does not oscillate, primarily because the elevator deflection reaches equilibrium once the desired altitude is reached.

Robustness of the VS observer is demonstrated by adding Gaussian noise with a standard deviation of 0.075 m/s to all body

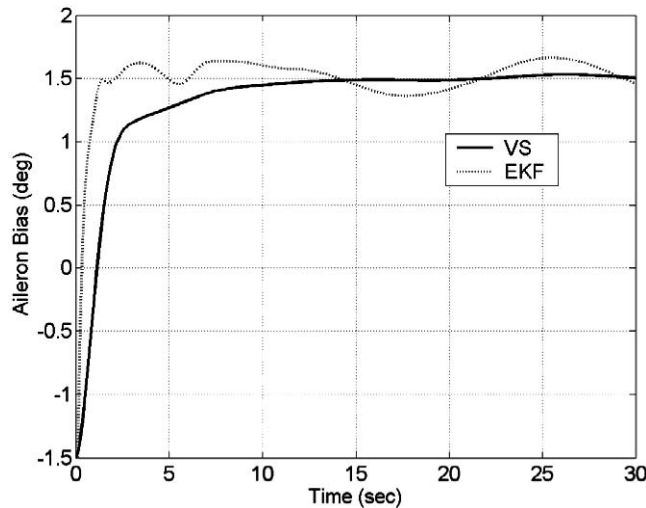


Fig. 1 Aileron bias with no sensor noise.

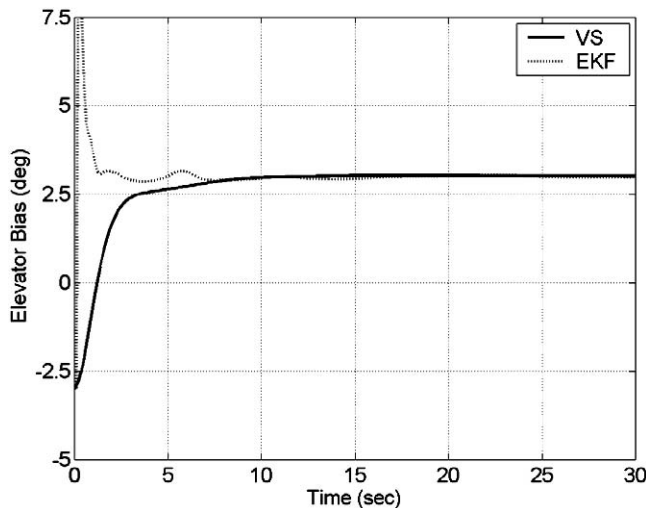


Fig. 2 Elevator bias with no sensor noise.

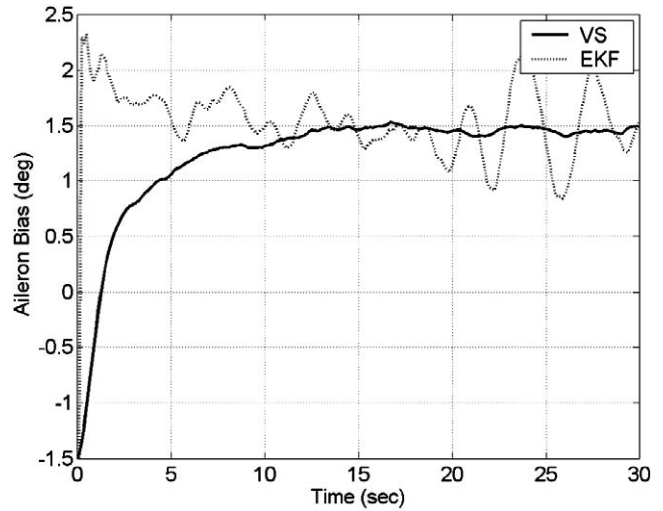


Fig. 3 Aileron bias with sensor noise.

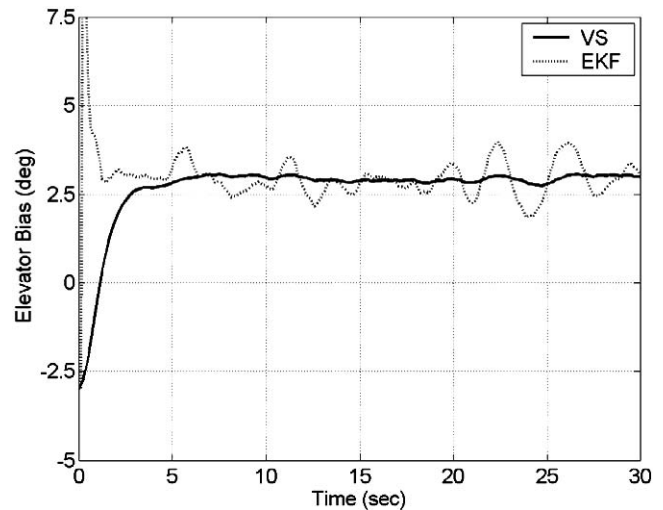


Fig. 4 Elevator bias with sensor noise.

velocities and noise with a standard deviation of 0.125 deg/s to all angular velocities. Model errors are introduced by altering all aerodynamic coefficients randomly by 5%. The parameters K_1 , K_3 , σ_1 , and σ_3 and the switching gains all remain the same. Figures 3 and 4 compare the VS observer to the EKF with sensor noise and model errors. The convergence time for the VS observer is the same with and without noise. Aileron bias estimation for the VS observer converges to the correct bias with only minor effects from noise and model error demonstrating robustness. The EKF, however, continues to wander around the true bias, just as in the case with no noise, but the model errors have amplified the problem. Similar results are shown in Fig. 4 for the estimated elevator bias in which the VS observer is insensitive to the noise and model errors, but the EKF estimation errors are amplified.

An added benefit of the VS observer is parameters that are free to select have obvious effects in the resulting observer. The four parameters K_1 , K_3 , σ_1 , and σ_3 all change the convergence rate, whereas the switching parameters change the robustness. The nonswitching parameters are limited only by their tendency to create “stiff” observer differential equation when K_1 and K_3 are large and σ_1 and σ_3 are small. In simulation, it was demonstrated that when using suitable gain parameters, even for a large integration interval of 0.125 s, the switching creates no problem for the VS observer. The EKF requires the measurement and model covariance as tuning parameters, with the latter often being difficult to quantify. Small changes in measurement and model covariance may lead to poor performance or instability.

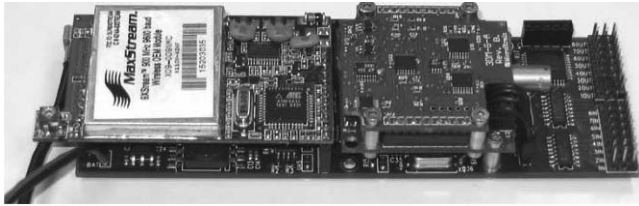


Fig. 5 Controller and sensor system.

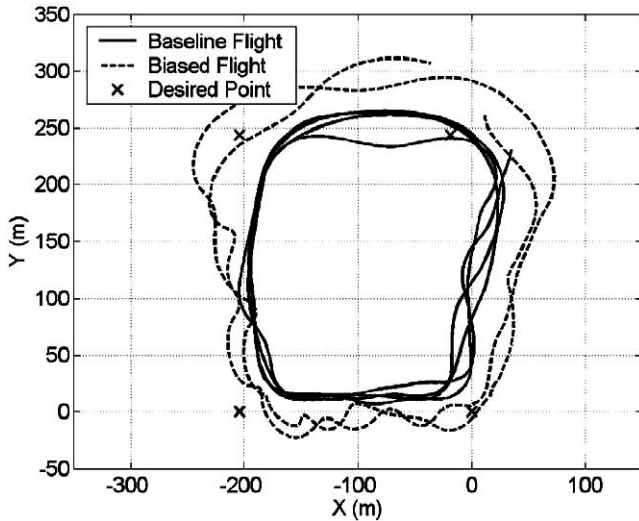


Fig. 6 Controlled UAV path.

The VS observer was flight tested on a RC trainer aircraft powered by a 40 series glow engine. The test aircraft has dimensions and mass properties described in Table 1. The aerodynamic coefficients in Table 2 were estimated using semi-empirical methods in Datcom [19]. A model-based controller was implemented to track desired points defined by their position and altitude. The sensor suit shown in Fig. 5 includes three single-axis ADXRS300 gyroscopes, two ADXL320 two-axis accelerometers, a HMC1053 three-axis magnetometer, and a 4-Hz GPS receiver. Two flights were completed: a baseline flight in which the aileron and elevator were visually aligned to minimize control surface bias and a biased flight in which 3 and 4 deg of aileron and elevator bias were added. Flight results are shown in Figs. 6 and 7. In Fig. 6 the desired path is defined by four points that create a square 200×250 m. The baseline flight

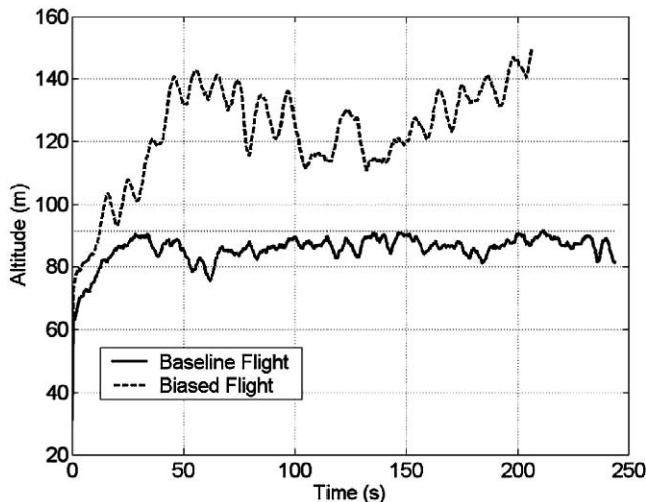


Fig. 7 Controlled UAV with desired altitude of 90 m.

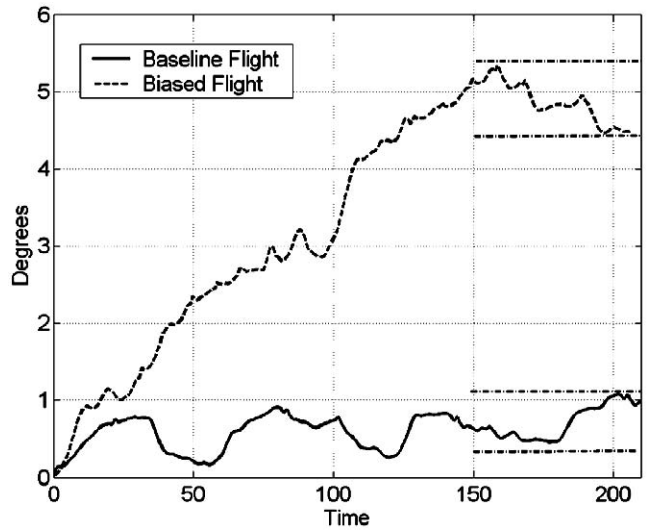


Fig. 8 VS elevator bias estimation.

performs well, tracking the desired path within 25 m however; when 3 deg of aileron bias is added, the UAV continually tries to roll away from the desired path and the error more than doubles. A similar result for a desired altitude of 90 m is shown in Fig. 7, in which the baseline flight has errors of less than 12 m, but when elevator bias is added, the UAV climbs 50 m above the desired altitude.

Results of the VS observer for the baseline and biased flights are shown in Figs. 8 and 9 for the elevator and aileron, respectively. The observer is numerically integrated at 16 Hz using a fourth-order Runge–Kutta algorithm in which course and ground speed from the GPS receiver are assumed constant between 4-Hz updates. The proportional observer gains K_1 and K_3 are 20, whereas the switching gains K_{S1} and K_{S3} are 5.0. Parameters σ_1 and σ_3 are chosen as 1684 and 1564, respectively. Finally, the matrices Q are chosen so that the solution to the Lyapunov equation for the systems in Eqs. (28) and (29) yields $p_{12}^1/p_{22}^1 = 0.0008$ and $p_{12}^2/p_{22}^2 = 0.0009$. Despite the attempt to eliminate all control bias for the baseline case, it can be seen that the VS observer estimates biases centered at 0.7 and -0.7 for the elevator and aileron, with the estimates converging within ± 0.40 and ± 0.25 deg, respectively, over the final 60 s of flight. Estimated biases for the biased flight are 4.9 deg for the elevator and 1.8 deg for the aileron, with estimates converging within ± 0.50 and ± 0.13 deg over the final 60 s. Total estimated bias added to the elevator and aileron during biased flight is then 4.2 and 2.5 deg, compared with the known biases of 4 and 3 deg.

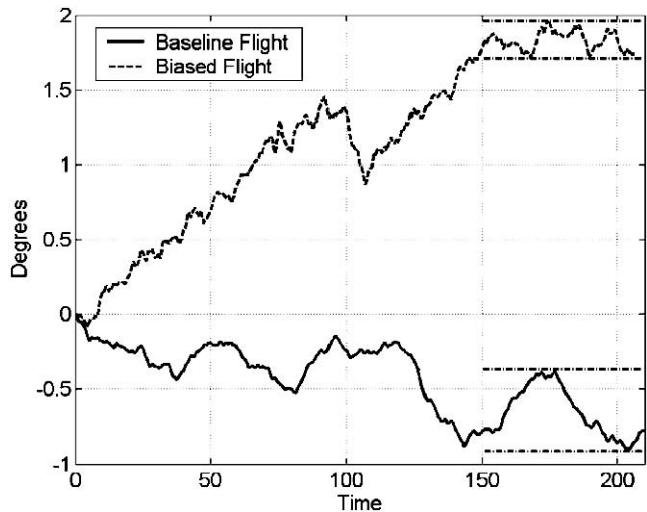


Fig. 9 VS aileron bias estimation.

V. Conclusions

A nonlinear observer has been developed to predict control surface bias on fixed wing unmanned air vehicles. Lyapunov theory is used to evaluate the region of practical stability when uncertainty is present. The observer is compared in simulation to an EKF, for which it is observed that the VS observer is robust to modeling noise. In comparison, the EKF aileron bias oscillates with the aileron deflection even without modeling errors. The presence of modeling errors further degrades the EKF performance. It is shown that the proposed observer is tolerant of low integration rates, in contrast to most switching controllers for which high switching frequencies are required. The VS observer is tested on a UAV, for which it is shown that small control biases can successfully be observed and could be used to increase tracking performance.

References

- [1] Steinberg, M. L., *A Comparison of Intelligent Adaptive Nonlinear Flight Control Laws*, Naval Air Development Center, Patuxent River, MD, 2001.
- [2] Chandler, P. R., Pachter, M., and Mears, M., "System Identification for Adaptive and Reconfigurable Control," *Journal of Guidance, Control, and Dynamics*, Vol. 18, No. 3, May–June 1995, pp. 516–524.
- [3] Bodson, M., "Reconfigurable Nonlinear Autopilot," *Journal of Guidance, Control, and Dynamics*, Vol. 26, No. 5, Sept.–Oct. 2003, pp. 719–727.
- [4] Ward, D., and Monaco, J., and Schierman, D., "Reconfigurable Control for VTOL UAV Shipboard Landing," *Proceedings of the AIAA Guidance, Navigation, and Control Conference*, AIAA, Reston, VA, 1999, pp. 499–509.
- [5] Shore, D., and Bodson, M., "Flight Testing of a Reconfigurable Control System of an Unmanned Vehicle," *Journal of Guidance, Control, and Dynamics*, Vol. 28, No. 4, July–Aug. 2005, pp. 698–707.
- [6] Shin, J. Y., Wu, N. E., and Belcastro, C., "Adaptive Linear Parameter Varying Control Synthesis for Actuator Failure," *Journal of Guidance, Control, and Dynamics*, Vol. 28, No. 4, July–Aug. 2005, pp. 698–707.
- [7] Unsal, C., and Kachroo, P., "Sliding Mode Measurement Feedback Control for Antilock Braking," *IEEE Transactions on Control Systems Technology*, Vol. 27, No. 5, Sept.–Oct. 2004, pp. 787–794.
- [8] Crassidis, J., and Lai, K., "Real-Time Attitude Independent Three-Axis Magnetometer Calibration," *Journal of Guidance, Control, and Dynamics*, Vol. 28, No. 1, 2005, pp. 115–120.
- [9] Bestle, D., and Zeitz, M., "Canonical Form Observer Design for Nonlinear Time-variable Systems," *International Journal of Control*, Vol. 38, No. 2, 1983, pp. 419–431.
- [10] Reboulet, C., and Champetier, C., "A New Method for Linearizing Nonlinear Systems: The Pseudolinearization," *International Journal of Control*, Vol. 40, No. 4, 1984, pp. 631–638.
- [11] Slotine, J.-J. E., Hedrick, J. K., and Misawa, E. A., "Sliding Observers for Nonlinear Systems," *Journal of Dynamic Systems, Measurement, and Control*, Vol. 109, Sept. 1987, pp. 245–252.
- [12] Canudas De Wit, C., and Slotine, J.-J. E., E. A., "Sliding Observers for Robot Manipulators," *Automatica*, Vol. 27, No. 5, 1991, pp. 859–864.
- [13] Misawa, E. A., and Hedrick, J. K., "Nonlinear Observers: A State-of-the-Art Survey," *Journal of Dynamic Systems, Measurement, and Control*, Vol. 111, No. 3, 1989, pp. 344–355.
- [14] Wang, G., Peng, S., and Huang, H., "A Sliding Observer for Nonlinear Process Control," *Chemical Engineering Science*, Vol. 52, No. 5, 1997, pp. 787–805.
- [15] Benhaib, A., Rachid, A., Audrezet, E., and Tadjine, M., "Real-Time Sliding-Mode Observer and Control of an Induction Motor," *IEEE Transactions on Industrial Electronics*, Vol. 46, No. 1, Feb. 1999, pp. 128–138.
- [16] Zhan, Y. J., Chan, C. C., and Chau, K. T., "A Novel Sliding-Mode Observer for Indirect Position Sensing of Switched Reluctance Motor Drives," *IEEE Transactions on Industrial Electronics*, Vol. 46, No. 2, Apr. 1999, pp. 390–397.
- [17] Derdiyok, A., "Speed-Sensorless Control of Induction Motor Using Continuous Control Approach of Sliding-Mode and Flux Observer," *IEEE Transactions on Industrial Electronics*, Vol. 52, No. 4, Aug. 2005, pp. 1170–1176.
- [18] Edwards, C., and Spurgeon, S., *Sliding Mode Control, Theory and Applications*, Taylor and Francis, Bristol, PA, 1999, pp. 21–25.
- [19] Hoak, D. E., Ellison, D. E., and Finck, R. D., "The USAF Stability and Control Datcom," U.S. Air Force Wright Aeronautical Labs. Rept. TR-83-3048, Oct. 1960 (rev. 1978).